Int. J. Electrochem. Sci., 10 **(2015)** 9586 - 9604

International Journal of
ELECTROCHEMICAL
SCIENCE
www.electrochemsci.org

The Effects of Magnesium Particles in Mg-rich Primers Applied on AZ91D Magnesium Alloy

Xiangyu Lu[1,2], *Yu Zuo*[1,*], *Xuhui Zhao*[1], *Shangyi Shen*[1]

[1] Beijing Key Laboratory of Electrochemical Process and Technology for Materials, Beijing University of Chemical Technology, Beijing 100029, China
[2] School of Materials Science and Engineering, Jiangsu University of Science and Technology, Zhenjiang 212003, China
[*]E-mail: zuoy@mail.buct.edu.cn

Received: 26 August 2015 / *Accepted:* 15 September 2015 / *Published:* 30 September 2015

The effects of Mg particles in a Mg-rich epoxy primer (MRP) for AZ91D alloy was studied with electrochemical techniques. As the Mg content in the MRP increases, the electrochemical activity of the coating increases and the AZ91D alloy substrate is protected cathodically by the coating to some extent. However, the pore resistance of the coating decreases with the Mg content. As the result, the MRP with about 50% Mg content provides the longest protection time for AZ91D alloy. With a 50% Mg-rich coating, the AZ91D substrate could be cathodically polarized by about 100 mV, leading to obviously reduced corrosion rate. On the defect area of the coating, MRP also provides cathodic protection for the substrate for certain time, and the precipitation of $Mg(OH)_2$ on the defect area could provide barrier protection to the substrate to some extent. A three stage mechanism for the effects of MRP on AZ91D substrate is suggested.

Keywords: AZ91D Alloy; Magnesium; Coating; EIS; protection

1. INTRODUCTION

Magnesium alloys have a good application prospect in automotive, aerospace and other industries because of their good formability and high specific strength. However, the poor corrosion resistance of magnesium alloys limit their engineering applications [1-2]. As one of the main corrosion protection methods, coatings are widely used in the engineering applications. Apart from the barrier effect, the cathodic protection could be provided for the substrates by adding the active pigments in coatings. For protection of steels, this concept is well established in the design of zinc-rich primers and

has been well applied [3-13]. Protection by these primers is afforded primarily by sacrificial anode-based cathodic protection and secondarily by the precipitation of zinc hydroxide at bare sites [3,5,12,13]. Battocchi and co-workers have recently studied the protection mechanism of Mg-rich primers (MRP) on aluminum substrate [14-25]. The electrochemical behavior of MRP on aluminum alloys was investigated and the results showed that the protection mechanism of MRP on the Al substrate was divided into two stages. In the first stage, cathodic polarization prevented corrosion of aluminum, while in the later stage corrosion was further inhibited by the precipitation of the magnesium oxides. The localized techniques were also used to investigate the mechanism of cathodic protection of MRP on Al substrates. The results showed that both pit nucleation and the growth of the pre-existing pits on the Al substrates were prevented by the cathodic protection of magnesium [17-19]. Maier and Frankel [24] investigated the electrochemical behavior of MRP on AA2024-T3. It was reported that the cathodic protection of the MRP to act as a sacrificial anode for aluminum requires an activation time and the ability of MRP to protect the aluminum substrate depends on the area ratio of the coated/bare aluminum surface [24]. In addition, basic corrosion of AA2024-T3 possibly occured for samples connected with MRP due to the cathodic polarization of the aluminum surface [24]. During cathodic polarization, the pH will increase locally at the AA2024-T3 alloy surface, leading to dissolution of aluminum oxide and the resultant loss of passivity [24]. King and Scully further studied the sacrificial and barrier protection mechanisms of the MRP on the AA2024-T351 substrate [25]. The authors developed two possible protection modes: long-range protection of remote defects and local or short-range Mg pigment-based protection of local and buried defects [25].

Among structural materials, magnesium is the most active in the electrochemical activity. Yet, Al, Zn and other alloy elements are usually included in engineering Mg alloys, leading to more positive potential than pure magnesium [26]. A pure magnesium (99.9%) film was made on AZ91D substrate using physical vapor deposition by Yu et al. [27]. It was reported that the magnesium film could protect the substrate as a distributed sacrificial anode [27]. In our previous work the epoxy coatings with addition of pure magnesium particles were applied on AZ91D substrates [28-33]. The open circuit potential (OCP) results showed that the OCP of AZ91D subatrate with MRP was more electronegative than that of bare AZ91D alloy in 3 wt% NaCl solution [28], suggesting cathodic protection of AZ91D alloy by the MRP. Meanwhile, it was shown that the MRP provided better protection for the AZ91D alloy than the epoxy coating without magnesium particles in the cross scratch testing [28]. The formation of $Mg(OH)_2$ in the MRP could provide barrier protection to some degree [28]. However, the potential difference (~120 mV in 0.1 wt% NaCl solution [28]) between pure magnesium and AZ91D is smaller than that between zinc and steel and even smaller after the magnesium particles are embedded in epoxy polymer. As is well known, a great enough potential difference is necessary for an effective cathodic protection. Hence, the electrochemical effect between the MRP and the AZ91D alloy substrate and the related mechanism are still to be further confirmed. In this work, the protection effect of Mg-rich epoxy primers with different Mg contents has been studied with EIS and OCP measurements. The protection mechanism of MRP on AZ91D substrate was studied.

2. EXPERIMENTAL

2.1. Materials

Yingkou galaxy magnesium aluminum Co., Ltd, China provided the AZ91D alloys. Table 1 shows the chemical compositions. A two component commercial epoxy (KFH-01) was used and obtained from Shijiazhuang Golden Fish Paint Company, China. Beijing Antepuna Trade Co., Ltd, China provided γ-glycidoxy propyl trimethoxysilane (γ-GPS). Qinhuangdao TaijiNano Products Co., Ltd, China produced the pure magnesium particles (99.9%). The size distribution of Mg particles was measured with a laser particle analyzer (Mastersizer 2000, Malvern Instruments Ltd., UK). The result yields an average Mg particle size of 21 μm， and the size range is approximately 6-50 μm.

Table 1. Chemical compositions (wt%) of AZ91D alloy

Al	Mn	Zn	Fe	Si	Ni	Cu	Mg
9.4	0.23	0.82	0.005	0.01	0.002	0.02	remainder

2.2. Samples preparation

AZ91D alloys were cut into the 50 × 50 × 3 mm size of panels. The panels were polished with 240# SiC abrasive papers, washed in deionized water and then acetone, and finally blown dry by cold air.

MRP with varying PVCs (pigment volume concentrations) were prepared first by adding Mg particles into the epoxy component. The PVC of every MRP was adjusted to reach a magnesium content in dry coating from 40 percent to 70 percent with an increment of 10 percent. Table 2 shows the labels of the different MRPs. As dispersing agent, the γ-GPS was added into the MRP at 1% w/w relative to the Mg particles weight. The Mg particles were dispersed by a high speed mixer. After 10 min of dispersion, the polyamide component was added at the weight ratio of 3:10 with respect to the epoxy. Then the MRP was prepared on AZ91D panels with manual brushing. The coated samples were placed indoors for one week in order to dry. A digital thickness gauge TT230 was employed to measure the MRP thickness and of the thickness was 130 μm (±10 μm).

Table 2. The tested Mg-rich primers with different Mg contents

Label	PVC (%)	Mg content to dry film (%)
MRP40	33.2	40
MRP50	42.7	50
MRP60	52.8	60
MRP70	63.5	70

2.3. Electrochemical tests

The 1000# SiC abrasive papers were applied to abrade AZ91D alloy and pure magnesium used in the electrochemical tests.

A PARSTAT 2273 workstation (Princeton applied research CO. Ltd, USA) was used in electrochemical impedance spectroscopy (EIS) measurements, over the frequency range from 100 kHz to 0.01 Hz (30 points measured, 4 steps per decade), with a 10 mV potential perturbation. A less than 5 pF internal capacitance is parallel in the instrument. A three-electrode system was adopted, in which the reference electrode was a saturated calomel electrode (SCE), the counter electrode was a platinum electrode, and the working electrode was the tesed sample. For MRPs coated AZ91D alloys, EIS tests were performed within 3 wt% NaCl solution under open circuit potential. The tested solution was refreshed every 24 h. For bare AZ91D alloy, EIS measurement was performed in 0.05wt% NaCl solution at different potentials and the working electrode area was 1 cm^2. ZSimpWin software was used to fit the impedance spectra.

a CS300 electrochemical system (Corrtest, Beijing, China) was empolyed to measure the galvanic current between the MRP sample and the bare AZ91D substrate in 3 wt% NaCl solution. In the testing system, the MRP sample with 7.0 cm^2 of eposed area was one working electrode, the bare AZ91D substrate with 0.01 cm^2 of exposed area (simulating a coating defect) was the other electrode, and a SCE was the reference electrode.

The CS300 electrochemical system was used to measure the potentiodynamic polarization plots of the pure magnesium, the bare AZ91D substrate and the MRP samples in 0.05 wt% NaCl solution (pH=7). A SCE was the reference electrode, a Pt electrode was the counter electrode, and the working electrode area was 1 cm^2. For the pure magnesium sample and the bare AZ91D substrate, after 10 min of immersion in the tested solution, the potentiodynamic polarization was performed from −200 mV (relative to the OCP) to the anodic direction with a rate of 0.2 mV/s. For the MRP coated AZ91D alloy samples, after 7 days of immersion in the tested solution, the potentiodynamic polarization was performed with a rate of 1 mV/s. The OCP for the MRP coated AZ91D alloy was measured in 3 wt% NaCl solution.

2.4. Scanning electron microscope (SEM)

The morphology of the MRP coated AZ91D alloy was characterized by a field emission scanning electron microscope (Hitachi S4700) with 20 kV of operating potential. The tested samples were treated by spray-gold to achieve good conductivity in measurement.

3. RESULTS AND DISCUSSION

3.1. EIS measurement

Fig. 1a shows the EIS spectra for MRP40 coated AZ91D panels. Within 1-168 h of immersion, a partial semi-circle was observed in the Nyquist plot, and the low frequency (0.01 Hz) impedance, $|Z|$, was higher than $10^{11}\ \Omega\ cm^2$, suggesting that the coating showed a classical barrier behavior. With the

immersion time prolonging, the decreasing diameter of the semi-circle showed the electrolyte absorption of the coating.

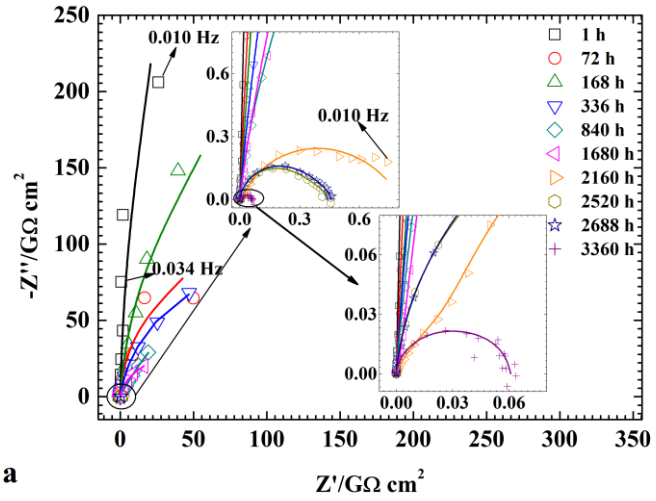

a

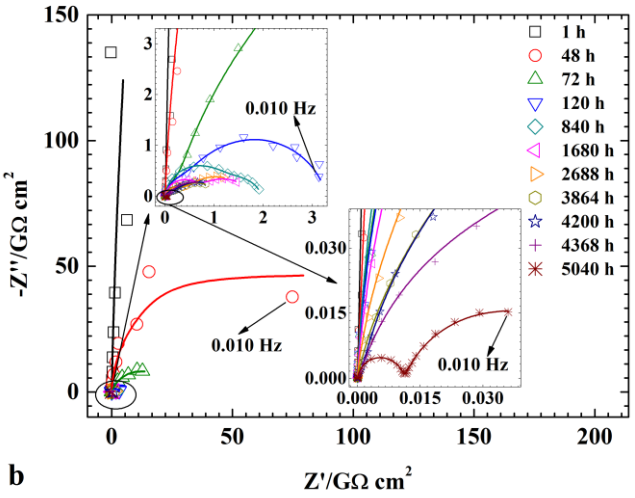

b

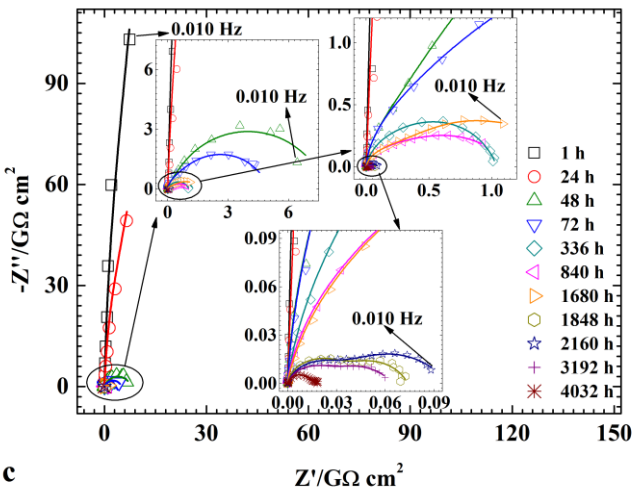

c

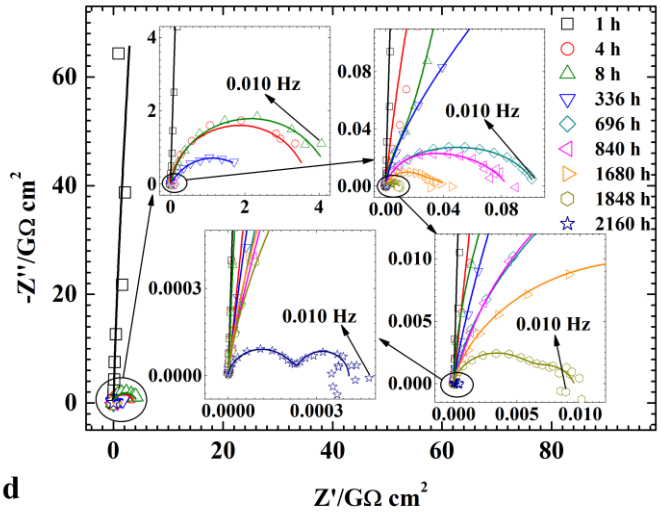

Figure 1. Impedance spectra and fitting curves for AZ91 alloy with MRPs as function of immersion time in 3 wt% NaCl solution: dot—experimental data, line—fitting results; a) MRP40, b) MRP50, c) MRP60, d) MRP70.

From 336 h to 1680 h, only one semi-circle was obtained and the slowly decreasing |*Z*| value (0.01 Hz) indicated that the protective performance of the MRP was stable. After 2160 h of exposure time, the second semi-circle appeared in the low frequency range and the |*Z*| value (at 0.01 Hz) decreased obviously, showing gradual degradation of the coating. After immersion for 3360 h, the Nyquist plot presented a scattered tail, implying that corrosion process happened at the substrate/coating interface on the coating defect [6, 7, 30].

Fig. 1b shows EIS results for the MRP50 coated panels in 3 wt% NaCl solution. Similar to the results of MRP40 coated sample, a barrier behavior was obtained for MRP50 samples at the beginning of immersion (1-48 h). Then, the |*Z*| value (0.01 Hz) decreased gradually because of the electrolyte absorption of the coating. From 120 h to 4368 h, there was no large evolution in the impedance spectra and the |*Z*| value (0.01 Hz) decreased slowly, suggesting that the MRP protective performance was stable. After immersion for 5040 h, a large decrease of |Z| value appeared in Fig. 1b, revealing the failure of MRP50 [28-30].

The EIS spectra for MRP60 and MRP70 are presented in Fig. 1c and Fig. 1d, respectively. For MRP60, a barrier behavior was obtained in immersion time from 1 to 24 hours. From 48 h to 3192 h, the impedance value of MRP60 decreased gradually due to the electrolyte absorption of the MRP60 and the magnesium particles activation. After immersion for 4032 h, a tail parallel to the real axis was observed in the Nyquist plot (Fig. 1c), implying the MRP60 failure [28-30]. From Fig. 1d, it could be seen that the barrier behavior of MRP70 maintained only during the initial immersion. After immersion for 2160 h, an inductive loop was observed in the low frequency domain and the |Z| value (0.01 Hz) was lower than $10^6\ \Omega\ cm^2$, showing the MRP70 failure.

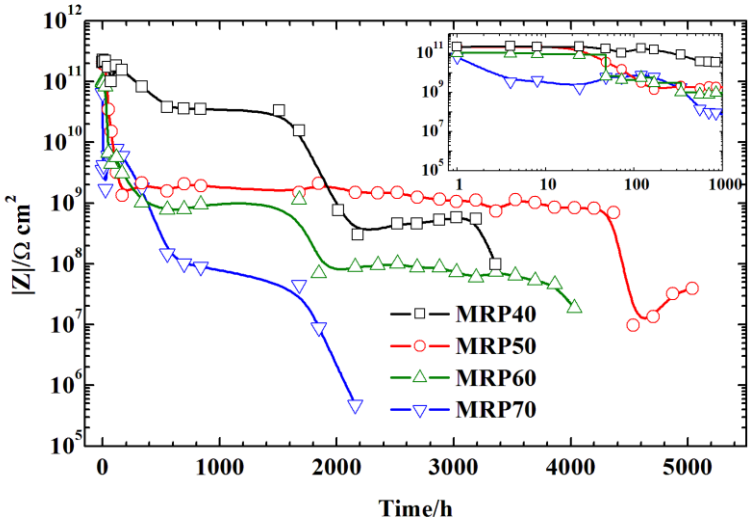

Figure 2. The variations of |Z| values (0.01 Hz) with immersion time in 3 wt% NaCl solution.

Fig. 2 shows the variations of the |*Z*| values (0.01 Hz) of the MRP samples with various immersion time. For all the samples, the |*Z*| values (at 0.01 Hz) were near 10^{11} Ω cm^2 in the initial immersion time, indicating the barrier properties of the primers. Then, the |*Z*| values decreased gradually resulting from the electrolyte absorption of MRPs and the activation of pure magnesium particles. After 552 h of immersion, the |*Z*| values of MRP40, 50, 60 and 70 dropped to 10^{10}, 10^9, 10^8 and 10^7 Ω cm^2, respectively. This phenomenon indicates that the increase in Mg content in the coating decreased the barrier protection efficiency. With the immersion time prolonging, the |*Z*| value of the MRP coated samples decreased slowly, indicating that the pores or capillary channels in the MRPs increased. After immersion for 1680 h, the |*Z*| values of MRP40, 60 and 70 samples declined significantly, implying the deterioration of the MRPs. However, for MRP50 sample there was almost no change in the |*Z*| values from 552 h to 4368 h of immersion. After 2160 h of immersion, the |*Z*| value for MRP70 was lower than 10^6 Ω cm^2, indicating the coating failure. For MRP40 sample, the |*Z*| value showed another decrease after 3192 h of immersion. Meanwhile, according to the Nyquist plot the MRP40 coating failed after 3360 h of immersion (Fig. 1a). The |*Z*| value of MRP50 did not decrease until 4536 h of immersion and the AZ91D alloy substrate did not show obvious corrosion until 5040 h of immersion (Fig. 1b). For MRP60 sample, the |*Z*| value kept stable until 4032 h of immersion. Therefore, among all the samples MRP50 provided the longest protection time. The increase of Mg content in the coating reduced the lifetime of the coating when Mg content was above 50%.

In order to get more accurate fitting results, the constant phase elements, *Q*, was used to fit the capacitive responses. *Q* is defined as

$$Z_Q = \frac{1}{Y_0(j2\pi f)^n} \quad (1)$$

in which $j = \sqrt{-1}$, f is the frequency (Hz), Y_0 is the CPE constant, the exponent n is equal to $\alpha/(\pi/2)$, and α *is* the phase angle of *Q* (radians) [30].

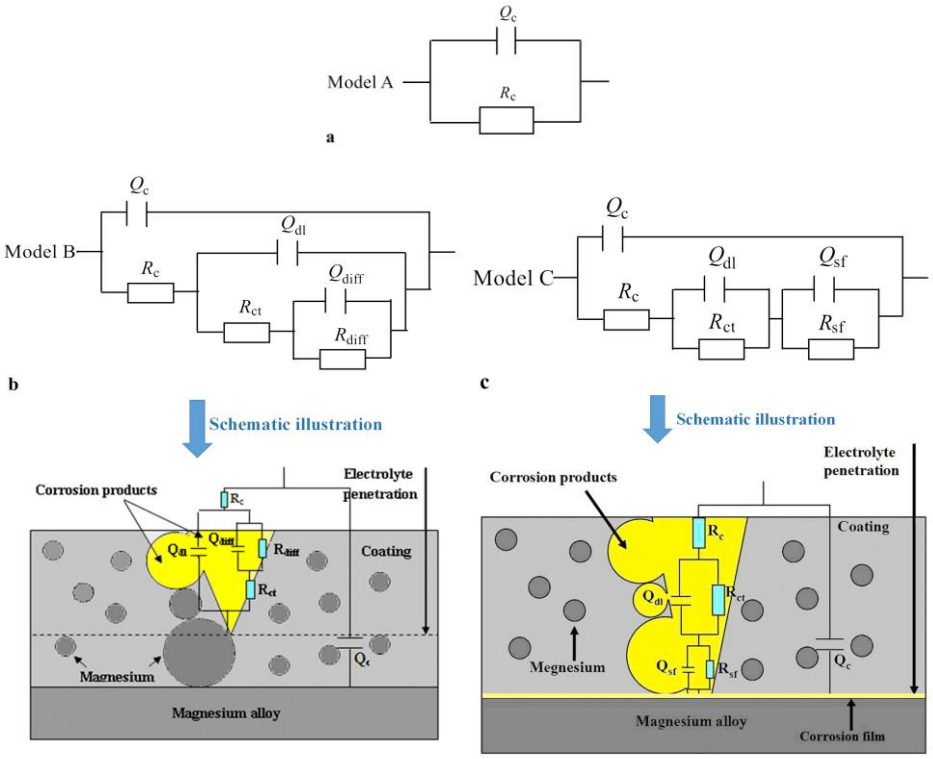

Figure 3. Equivalent electrical circuits used to fit EIS results: a) initial stage, b) stable stage, c) late stage.

The EIS results were fitted to the electrical equivalent circuits (EEC) (Fig. 3) used in the previous studies [28-30] for AZ91D substrates with MRP. In the initial immersion stage, a simple EEC, as shown in Fig. 3a, can be adopted to fit the EIS results. In model A, Q_c is the coating capacitance and R_c is the coating resistance. Good fitting results were obtained for MRP40 within 1-168 hours (Fig. 1a), for MRP50 within 1-48 hours (Fig. 1b), for MRP60 within the 1-24 hours (Fig. 1c) and for MRP70 within 1-4 hours (Fig. 1d).

Then, after a period of immersion, model B (Fig. 3b), proposed by Battocchi et al, could be used to explain the EIS spectra. In model B Q_c is the coating capacitance and R_c is the coating resistance, while Q_{dl} is the double-layer capacitance at the interface between Mg particles and electrolyte and R_{ct} is the charge-transfer resistance of the Mg particles. The precipitation of corrosion products of magnesium particles could cause diffusion processes, which was explained by the capacitance Q_{diff} in parallel to the resistance R_{diff}, noted as Z_{diff} [7, 28-30, 34]. In this study, the values of the exponent n in Q_{diff} from model B fluctuate from 0.3 to 0.5 with immersion time, suggesting that the Z_{diff} is probably related to finite-layer diffusion [7, 28-30, 34]. Model B provides good fitting results for MRP40 within 336-2520 hours (Fig. 1a), for MRP50 within 72-4200 hours (Fig. 1b), for MRP60 within 48-1680 hours (Fig. 1c) and for MRP70 within 8-696 hours (Fig. 1d).

Fig. 3c presents the schematic representation of the physical meaning of model C. Model C is composed of the coating capacitance Q_c, the coating resistance R_c, the charge-transfer resistance of the Mg particles R_{ct} , the double-layer capacitance at the interface of Mg particles/electrolyte Q_{dl}, and

($R_{sf}C_{sf}$), caused by the lateral diffusion of the electrolyte at the substrate/coating interface [30, 35, 36]. In addition, when corrosion occurs on the alloy substrate, the corrosion products of the substrate would form a film [30, 34, 37]. Then, R_{sf} is the film resistance and C_{sf} is the film capacitance [30, 34, 37]. Hence, the EIS spectra could be fitted using Model C for MRP40 within 2688-3360 hours (Fig. 1a), for MRP50 within 4368-5040 hours (Fig. 1b), for MRP60 within 1848-4032 hours (Fig. 1c) and for MRP70 within 840-2160 hours (Fig. 1d).

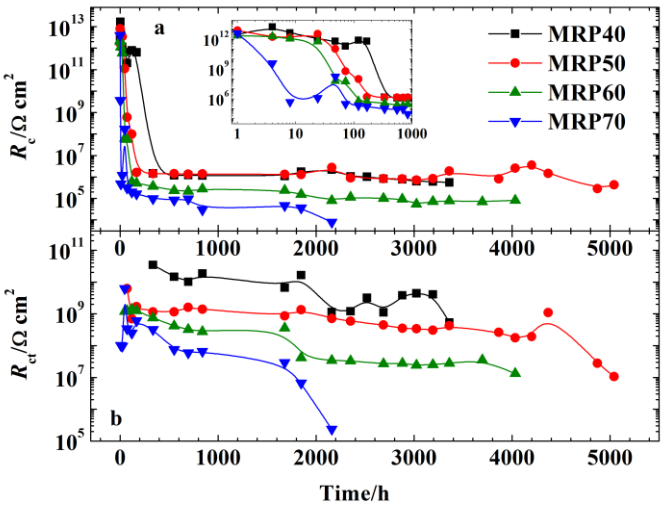

Figure 4. The variations of the coating resistance R_c and the charge-transfer resistance R_{ct} with immersion time in 3 wt% NaCl solution.

Fig. 4 shows the variations of the coating resistance R_c and the charge-transfer resistance R_{ct} with immersion time. R_c is an indication of the deterioration and porosity of coatings [30, 38, 39]. R_c can be associated with the number of pores or capillary channels in the coating [38, 39]. R_c is defined as:

$$R_c = \frac{d}{\kappa N A_c} \qquad (2)$$

in which κ is the electrolyte conductivity, N is the channels number, A_c is the average cross-section area of the permeability channels, and d is the channel length, which is equal to the thickness of coating. During the initial immersion, the R_c values of all the primers presented obvious decrease (Fig. 4a) due to the electrolyte permeation and the increase of capillary channels or pores in MRPs [30, 38, 39]. As the coating is saturated with water, a proper ionic conduction path formed through the coating in the process of electrolyte immersion [13]. Then, the R_c values maintained relatively stable, suggesting that the water permeation in the primers had reached the saturation limit. It could be seen that an increase in Mg content of the coating decreased the time for the primer to reach the saturation limit, that is, decreased the pore resistance of the coating.

R_{ct} is a measure of the electrochemical reaction activity of the Mg particles and the interface stability of Mg particles/resin [15, 28, 30]. In initial time, a thin layer of magnesium oxide covered the

surface of Mg particle. As water permeated in the primer, the oxide dissolved leading to the increase of reactive area and the number of Mg particles exposed to water. Those factors caused R_{ct} decrease (Fig. 4b). It is observed that the R_{ct} of all MRPs decreased slowly with immersion time, especially for MRP70. On the other hand, it is seen that the electrochemical reaction activity of Mg particles in coatings increased as the Mg content of the coating increased, which could be explained by the increase in the porous property of the coatings. The electrolyte was easy to permeate in the coatings due to the porous property of the coatings.

3.2. Galvanic coupling measurements

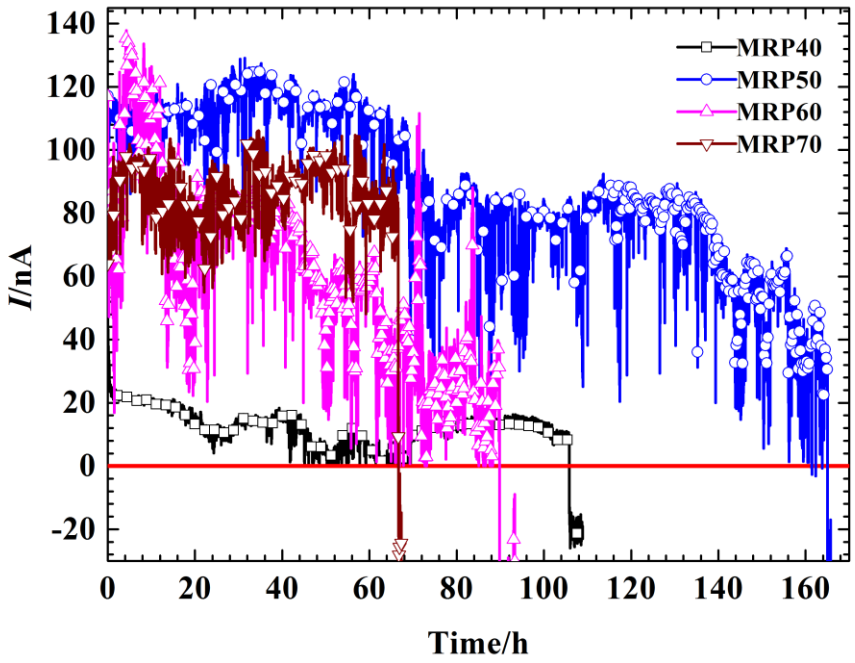

Figure 5. Galvanic currents of the bare AZ91D alloys coupled with different MRPs in 3 wt% NaCl solution.

Fig. 5 shows variations of the galvanic current for bare AZ91D alloy coupled with different MRP coated samples in 3wt% NaCl solution. When the current is positive, MRPs could provide cathodic protection to the bare AZ91D alloy. The galvanic coupling current of MRP40, 50, 60 and 70 remained positive values for about 105 h, 165 h, 90 h and 66 h, respectively. It could be found that the galvanic current value for the bare AZ91D alloy coupled with the MRP40 was lower than those for the bare AZ91D alloys coupled with the others (MRP50, 60 and 70). Hence a decrease in Mg content in the coating lead to lower galvanic current. However, the cathodic protection time provided by the MRP shortened rapidly when Mg content is higher than 50%.

3.3. Potentiodynamic polarization curves

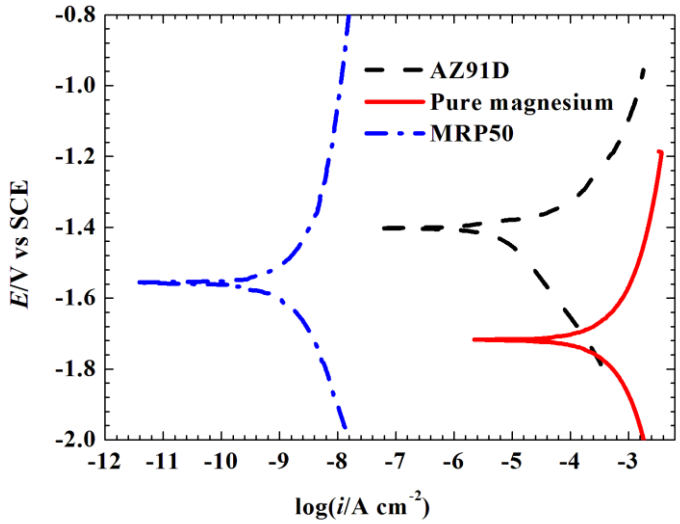

Figure 6. Polarization plots for pure magnesium, AZ91D alloy and MRP50 coated alloy in 0.05 wt% NaCl (pH=4) solution.

Table 3. The related parameters of the polarization plots for pure magnesium, AZ91D alloy and MRP50 in 3 wt% NaCl (pH=4) solution

Sample	E_{corr} (V vs SCE)	i_{corr} (A cm^{-2})	β_a (mV/decade)	β_c (V/decade)
Pure magnesium	-1.7174	6.5753×10^{-4}	458.58	485.45
AZ91D	-1.4025	2.3669×10^{-6}	36.857	76.83
MRP50	-1.5597	5.0696×10^{-9}	1441.6	845.79

The above results confirm that the MRP50 coating shows the best protection effect on AZ91D alloy. Fig. 6 shows the polarization plots of pure magnesium, AZ91D alloy and MRP50 coated AZ91D alloy in 0.05 wt% NaCl solution. Table 3 shows the related parameters obtained from Fg. 6 by extrapolation of the Tafel line. The corrosion rate of pure Mg is approximately 6.6×10^{-4} A cm^{-2} and the corrosion potential is about -1.7 V vs SCE. For AZ91D alloy, the corrosion rate of AZ91D alloy is about 2.4×10^{-4} A cm^{-2} and the corrosion potential is about -1.4 V vs SCE, about 300 mV higher than that of pure Mg. For the MRP50 sample, the corrosion potential is about -1.55 V vs SCE, about 150 mV lower than that of bare AZ91D alloy, suggesting that the MRP50 could cathodically polarize AZ91D alloy. The corrosion rate of the MRP50 coated sample is about 5.1×10^{-9} A cm^{-2}, indicating that the MRP50 slowed down the corrosion rate of AZ91D alloy by three orders of magnitude. Although usually in a galvanic couple the reactive rate of the more active metal is enhanced, the resin may decrease the reaction kinetic process of Mg particles leading to prolonging the protection lifetime.

For AZ91D alloy (the cathode), the reaction rate under charge-transfer control may be calculated using following equation [40]:

$$\frac{i_a^{Mg^{2+}}}{i_{corr}^{Mg^{2+}}} = \exp(-\frac{\Delta\varphi_c}{\beta_a}) \qquad (3)$$

where $i_a^{Mg^{2+}}$ is the current density of the anodic reaction occurring at the AZ91D electrode at different potentials, $i_{corr}^{Mg^{2+}}$ is the current density of the anodic reaction occurring at the AZ91D electrode at the corrosion potential, $\Delta\varphi_c$ is the cathodic over-potential of AZ91D alloy in solution, and β_a is the Tafel slope of the anodic dissolution reaction occurring on the AZ91D electrode. The value of β_a is 36.80 mV when AZ91D alloy was immersed in 0.05 wt% NaCl (pH=4) solution, by fitting the polarization curve of AZ91D alloy in Fig. 6. It may be calculated according to equation (3) that $i_a^{Mg^{2+}} / i_{corr}^{Mg^{2+}}$ would be 0.0660 when $\Delta\varphi_c$ is 100 mV. This means that the corrosion current density of the anodic dissolution reaction occurring at the AZ91D electrode is reduced to 6.60% of the $i_{corr}^{Mg^{2+}}$ value when the AZ91D alloy is cathodically polarized by 100 mV in 0.05 wt% NaCl (pH=4) solution.

3.4. The acting mechanism of magnesium particles in MRP

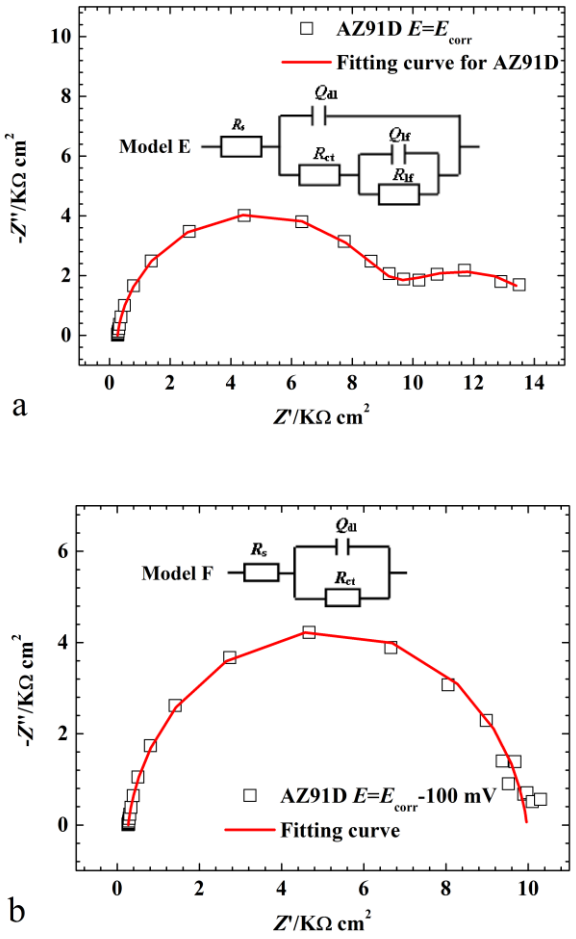

Figure 7. EIS spectra for AZ91D alloy in 0.05 wt% NaCl solution at different applied potentials: a) $E=E_{corr}$; b) $E=E_{corr}$-100mV.

Fig. 7 displays the Nyquist plots for AZ91D alloy at different applied potentials in 0.05% NaCl solution. At the corrosion potential, two capacitive loops are seen (Fig. 7a). The capacitive loop near the high frequency end may be reflected by a resistor in parallel with a double layer capacitor. Another time constant is observed is in the low frequency, probably because of mass transfer control at the corrosion spots. As shown in Fig. 7a, the EIS result can be fitted well by the EEC model D, in which R_s is the electrolyte resistance, Q_{dl} is the double layer capacitance on the AZ91D alloy/electrolyte interface and R_{ct} is the charge-transfer resistance of AZ91D alloy. The capacitance Q_{lf} in parallel to resistance R_{lf} is correlated to the mass transfer control process at the corrosion spots. At the cathodic potential (Fig. 7b), the Nyquist plot shows only one capacitive loop. The EIS spectra could be explained by Model E (Fig. 7b), in which R_s is the electrolyte resistance, R_{ct} is the charge-transfer resistance of AZ91D alloy and Q_{dl} is the double-layer capacitance at the AZ91D alloy/electrolyte interface. Then, the mass transfer control processes at the corrosion spots disappeared when the AZ91D sample was cathodically polarized by 100 mV.

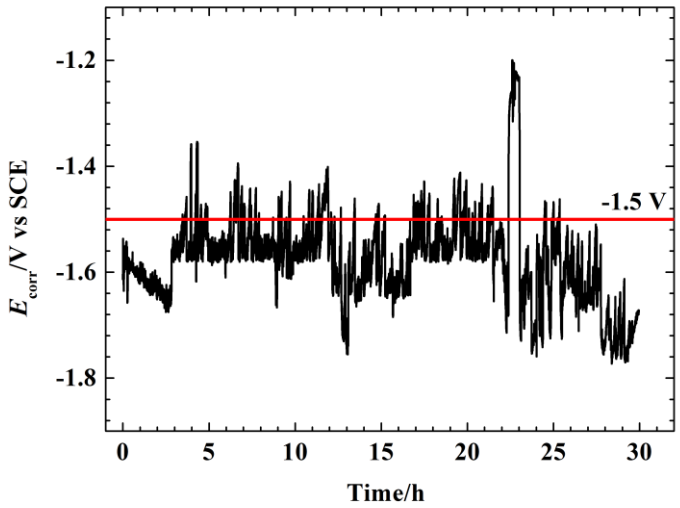

Figure 8. The corrosion potential E_{corr} of scratched MRP50 coated panel with immersion time in 3 wt% NaCl solution.

A MRP50 coated sample was scratched by a blade and the scratch is 0.5 cm long, 0.08 mm wide and deep to the substrate. The OCP was measured to further confirm the effect of cathodic protection of MRP on AZ91D substrate. Fig. 8 shows the result. In our study, E_{corr} of AZ91D alloy was found to be −1.5 V vs SCE in 3 wt% NaCl solution. Fig. 8 shows that the scratched MRP50 coated AZ91D sample exhibited fluctuant OCP values in the range of −1.8 V vs SCE to −1.2 V vs SCE. However, in most of the time the OCP value was below −1.5 V vs SCE, suggesting that MRP50 could cathodically polarize the AZ91D alloy on the coating defect. This test again confirms that the MRP could retard the corrosion rate of AZ91D alloy substrate to some extent.

Fig. 9a shows the impedance spectra of a AZ91D alloy sample without coating in 3 wt% NaCl. In the initial immersion (1 h), an inductive loop was observed in the low frequency domain, suggesting

that severe corrosion happened on the alloy. As immersion time prolonged, the impedance value decreased. After 24 h of immersion, black corrosion spots were observed on the AZ91D alloy sample.

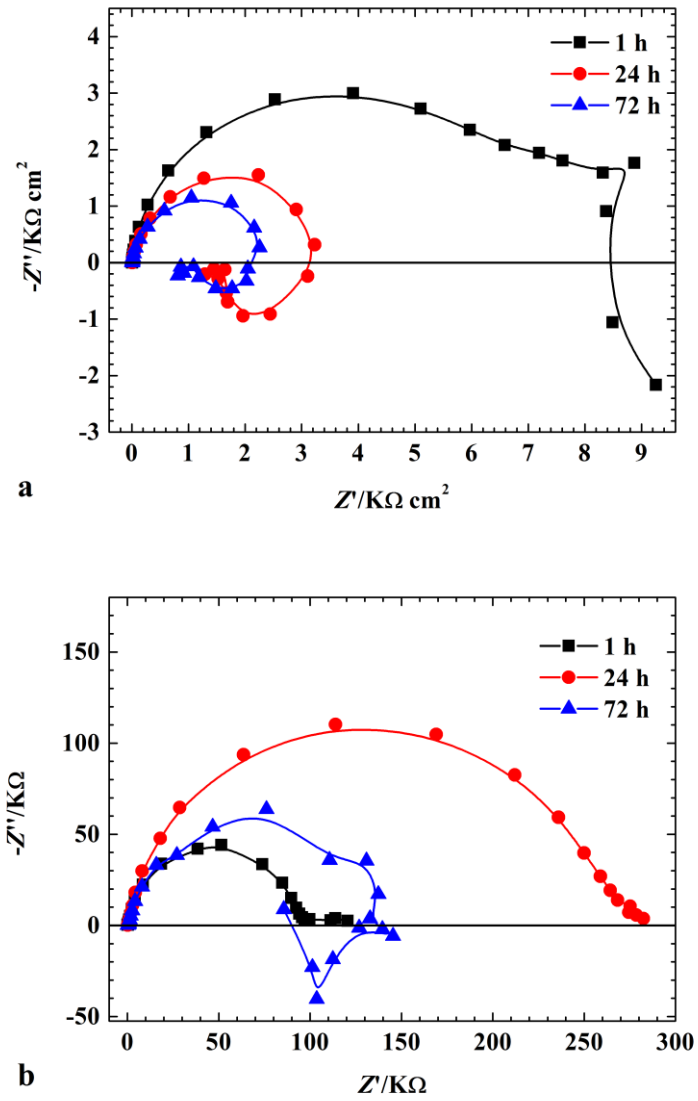

Figure 9. Impedance spectra of a) bare AZ91D alloy and b) AZ91D alloy sample coated with defected MRP50 at various exposure times in 3 wt% NaCl solution.

Further, on a MRP50 coated AZ91D sample, a defected area was induced with a knife tip, and the exposed area was approximately 0.001 cm^2. Fig. 9b shows the impedance spectra of the defected MRP50 coated AZ91D alloy with immersion time in 3 wt% NaCl. The impedance of this sample was comparatively small at the beginning, but increased with time in the first 24 h. After immersion for 24 h, the shape of the impedance spectra was similar to that of the impedance spectra (Fig. 7b) when the AZ91D sample was cathodically polarized by 100 mV, suggesting that the exposed substrate alloy at the defect area was cathodically polarized by the MRP50 coating. On the other hand, the increased impedance value means that the barrier property on the defected area was improved to some extent.

After 72 h of immersion, the Nyquist diagram (Fig. 9b) showed an inductive loop in the low frequency domain, indicating that the alloy was corroded severely. An inspection of the scribed area after 24 h of immersion by SEM revealed that a precipitation with needle-like loose structure existing on the defected area (Fig. 10), which was discerned as $Mg(OH)_2$ [28].

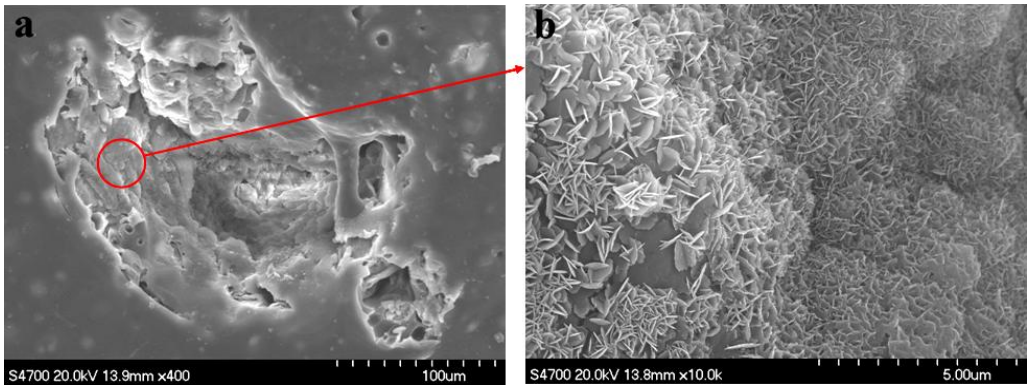

Figure 10. SEM micrograph of precipitates formed at a defect on MRP50 coated AZ91D alloy.

When magnesium particles and AZ91D alloy are coupled together, the magnesium particles behave as the anodic electrode and the AZ91D alloy as the cathodic electrode. Then, the anodic reaction mainly occurred on the Mg particle surface:

$$Mg \rightarrow Mg^{2+} + 2e \qquad (4)$$

Magnesium is active in a wide range of pH. Meanwhile, when pH is lower than 10.5, $Mg(OH)_2$ is not stable [41]. The cathodic reaction occurs mainly on the AZ91D alloy surface:

$$2H_2O + 2e \rightarrow 2OH^- + H_2\uparrow \qquad (5)$$

Therefore, the pH increse at the cathodic site, particularly at the coating defect area. Hence $Mg(OH)_2$ precipitates may form at the cathodic sites.

3.5. The variation of the corrosion potential

Fig. 11 presents the variations of the corrosion potential for AZ91D alloy with different MRPs in 3 wt% NaCl solution. The OCP values of all the samples could be divided into three periods according to the variations of the potential. From Fig. 11, it can be found that the effective cathodic protection time (the corrosion potential more negative than -1.5 V vs SCE) provided by MRP40, 50, 60 and 70 were about from 60 h to 130 h, 40 h to 700 h, 70 h to 240 h, and 10 h to 170 h, respectively. Therefore, the longest cathodic protection time was provided by MRP50，consistent with the results of galvanic coupling current measurement.

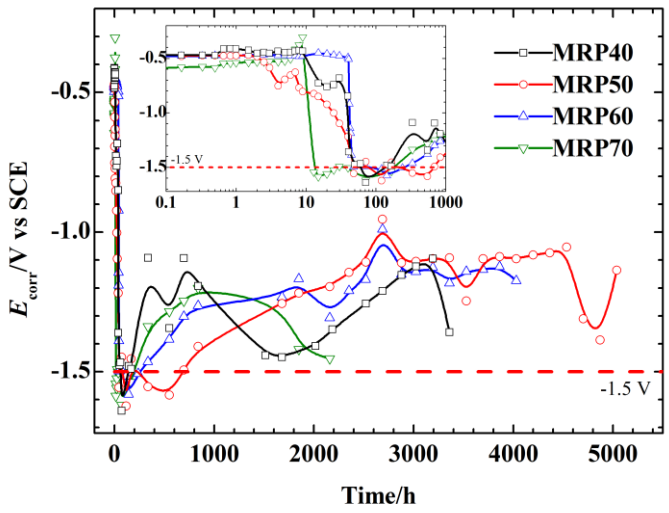

Figure 11. The variations of the corrosion potential for the different MRP samples with immersion time in 3 wt% NaCl solution.

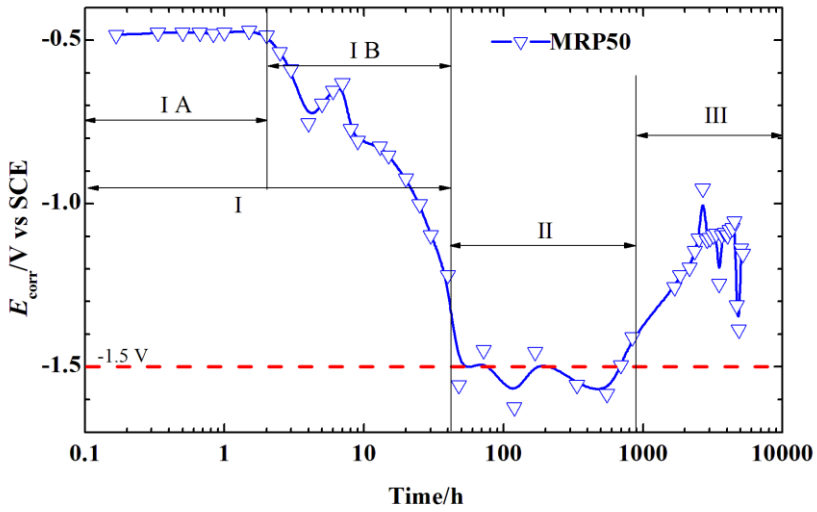

Figure 12. The variations of the corrosion potential for the MRP50 sample with immersion time in 3 wt% NaCl solution.

Fig. 12 presents the variations of the E_{corr} for MRP50 sample with immersion time in 3 wt% NaCl solution. The lifetime of the MRP50 could be divided into three main periods:

Period I: The E_{corr} decreased to the negative direction, until reaching −1.5 V vs SCE. The E_{corr} decreased in two different slopes. Based on the different slopes, period I is divided into two sub-periods: IA and IB.

Period II: The E_{corr} was lower than −1.5 V vs SCE, indicating that MRP50 provided cathodic protection for the AZ91D in this period.

Period III: After the cathodic protection period, the corrosion potential rose gradually over −1.5 V vs SCE, and fluctuated until the final failure of the coating.

In period IA, the corrosion potential remained relatively stable around −0.5 V vs SCE which may be because of the primer barrier property. The evolution of E_{corr} in period IB is caused by the changes of the area ratio of the active Mg particles to the AZ91D alloy substrate. The magnesium oxides originally covering the magnesium particles reacted with the permeated electrolyte, resulting in the establishment of electrical contact between the Mg particles and the AZ91D substrate. Then the magnesium particles were activated. Hence the area ratio of the active Mg particles to the AZ91D substrate increased continuously and the E_{corr} of the system decreased during period IB. Period II corresponds to the process during which the AZ91D alloy substrate was cathodically protected by the magnesium particles. In period III, the area ratio of magnesium particles to AZ91D alloy decreased due to corrosion of the magnesium particles. As mentioned previously, $Mg(OH)_2$ is not stable in water when pH value is lower than 10.5 [41]. However, with reduction of water and oxygen, the pH value increase quickly on cathodic sites due to the high electrochemical reactivity of Mg [15]. Therefore, as the Mg particles dissolved, $Mg(OH)_2$ precipitates formed in the MRP [28], leading to the increase of the E_{corr}. The formation of $Mg(OH)_2$ in MRP provides barrier protection to some extent, improving barrier property of the primer. It is worth to note in Fig. 12 that the period III occupied the longest time during the lifetime of the coating, which means that although the cathodic protection effect of Mg could extend the performance of the coating to some extent, the barrier effect of the corrosion products of Mg may have played a more important role in the whole lifetime of MRP.

From above study the protection provided by the MRP could be devided into three stages: In the first stage, the MRP shows barrier performance. In this stage the water permeation into the coating gradually activated and the Mg particles. In the second stage, the AZ91D alloy is cathodically protected. Under the studied condition the AZ91D substrate is cathodically polarized by about 100 mV and the corrosion rate is reduced obviously. The time length of the second stage is related to the consumption rate of the Mg particles available and the amount of Mg particles. This could be explained by that the increase in Mg content of the coating may introduce more pores and defects, thereby decrease the coating resistance. Then, the electrolyte is present in the whole coating with high Mg content soon after immersion. Hence the rapid accumulation of corrosion products around magnesium particles causes the rapid failure of the cathodic protection. Finally, in the third stage, the formation of the Mg corrosion products in the MRP leads to another barrier effect. In this stage, $Mg(OH)_2$ in the MRP strengthens the barrier performance of the coating. In addition, the precipitation of $Mg(OH)_2$ may also cover the defected spots on AZ91D alloy surface and provides additional barrier protection to the substrate to some extent.

4. CONCLUSIONS

(1) The EIS and potential measurement results show that, as the Mg content in MRP increases, the electrochemical reaction activity of the coating increases and the coating resistance decreases. As the result, the MRP with 50% Mg content provides the longest protection time for AZ91D alloy. Higher Mg content from 60% to 70% leads to rapid decrease of the coating performance.

(2) The galvanic current, OCP and polarization tests confirm the cathodic effect of MRP on AZ91D substrate. With a 50% Mg-rich coating, the AZ91D substrate could be cathodically polarized by about 100 mV, which would lead to obviously reduced corrosion rate for the AZ91D substrate.

(3) The effects of MRP on AZ91D alloy are proposed as follows: In the first stage, the MRP shows barrier effect. In this stage the water permeation into the coating gradually activated and the Mg particles. In the second stage, the substrate is cathodically protected by the Mg particles. Finally, formation of the Mg corrosion products in the coating again leads to barrier effect.

(4) At the defected areas of the coating, MRP also provides cathodic protection for the substrate for certain time, and the precipitation of $Mg(OH)_2$ on the defect area could provide barrier protection to the AZ91D substrate to some extent.

References

1. H. Inoue, K. Sugahara, A. Yananoto, *Corros. Sci*. 44 (2002) 603
2. W. Hou, Z. Kang, *Int. J. Electrochem. Sci*. 44 (2013) 5613
3. C.M. Abreu, M. Izquierdo, M. Keddam, X. R. Nóvoa, H. *Electrochim. Acta* 41 (1996) 2405
4. C.M. Abreu, M. Izquierdo, P. Merino, X. R. Nóvoa, C. Pérez, *Corrosion (Houston, TX, U. S.).* 55 (1999) 1173
5. H. Marchebois, S. Joiret, C. Savall, J. Bernard, S. Touzain, *Surf. Coat. Technol*. 157 (2002) 151
6. J.R. Vilche, E.C. Bucharsky, C.A. Giúdice, *Corros. Sci*. 44 (2002) 1287
7. H. Marchebois, M. Keddam, C.Savall, J. Bernard, S. Touzain, *Electrochim. Acta* 49 (2004) 1719
8. H. Marchebois, C. Savall, J. Bernard, S. Touzain, *Electrochim. Acta* 49 (2004) 2945
9. Ole Øystein Knudsen, U. Steinsmo, M. Bjordal, *Prog. Org. Coat*. 54 (2005) 224
10. D.P. Schmidt, B.A. Shaw, E. Sikora, W.W. Shaw, L.H. Laliberte, *Prog. Org. Coat.* 57 (2006) 352
11. L. Zhang, X.-Y. Lu, Y. Zuo, *Int. J. Electrochem. Sci.* 9 (2014) 6266
12. M. Yan, V.J. Gelling, B.R. Hinderliter, D. Battocchi, D.E. Tallman, G.P. Bierwagen, *Corros. Sci*. 52 (2010) 2636
13. S. Shreepathi, P. Bajaj, B.P. Mallik, *Electrochim. Acta* 55 (2010) 5129
14. M.E. Nanna, G.P. Bierwagen, *JCT research* 1 (2004) 69
15. D. Battocchi, A.M. Simões, D.E. Tallman, G.P. Bierwagen, *Corros. Sci*. 48 (2006) 1292
16. D. Battocchi, A.M. Simões, D.E. Tallman, G.P. Bierwagen, *Corros. Sci*. 48 (2006) 2226
17. A.M. Simões, D. Battocchi, D.E. Tallman, G.P. Bierwagen, *Corros. Sci*. 49 (2007) 3838
18. G. Bierwagen, D. Battocchi, A. Simões, A. Stamness, D. Tallman, *Prog. Org. Coat*. 59 (2007) 172
19. A. Simões, D. Battocchi, D. Tallman, G. Bierwagen, *Prog. Org. Coat*. 63 (2008) 260
20. G. Bierwagen, R. Brown, D. Battocchi, S. Hayes, *Prog. Org. Coat*. 67 (2010) 195
21. R.L. DeRosa, I. Szabo, G.P. Bierwagen, D. Battocchi, *Prog. Org. Coat.* 78 (2015) 455
22. S.S. Pathak, M.D. Blanton, S.K. Mendon, J.W. Rawlins, *Corros. Sci*. 52 (2010) 1453
23. J.-G. Wang, Y. Zuo, Y. -M. Tang, *Int. J. Electrochem. Sci.* 8 (2013) 10190
24. B. Maier, G.S. Frankel, *Corrosion (Houston, TX, U. S.).* 67 (2011) 055001
25. A.D. King, J.R. Scully, *Corrosion (Houston, TX, U. S.).* 67 (2011) 055004
26. G.-L. Song, A. Atrens, M. Dargusch, *Corros. Sci*. 41 (1999) 249
27. B.-L. Yu, J.-Y. Uan, *Scr. Mater*. 54 (2006) 1253
28. X.-Y. Lu, Y. Zuo, X.-H. Zhao, Y.-M. Tang, X.-G. Feng, *Corros. Sci*. 53 (2011) 153
29. X.-Y. Lu, Y. Zuo, X.-H. Zhao, Y.-M. Tang, *Corros. Sci*. 60 (2012) 165
30. X.-Y. Lu, Y. Zuo, X.-H. Zhao, Y.-M. Tang, *Electrochim. Acta* 93 (2013) 53
31. S.-Y. Shen, Y. Zuo, X.-H. Zhao, *Corros. Sci.* 76 (2013) 275
32. S.-Y. Shen, Y. Zuo, *Corros. Sci.* 87 (2014) 167

33. X.-Y. Lu, X.-G. Feng, Y. Zuo, C.-B. Zheng, S. Lu, L. Xu, *Surf. Coat. Technol*. 270 (2015) 227
34. J.-T. Zhang, J.-M. Hu, J.-Q. Zhang, C.-N. Cao, *Prog. Org. Coat*. 51 (2004) 145
35. C.I. Elsner, E. Cavalcanti, O. Ferraz, A.R. Di Sarli, *Prog. Org. Coat*. 48 (2003) 50
36. B. del Amo, L. Véleva, A.R. Di Sarli, C.I. Elsner, *Prog. Org. Coat*. 50 (2004) 179
37. J.-M. Hu, J.-Q. Zhang, C.-N. Cao, *Prog. Org. Coat*. 46 (2003) 273
38. M. Kendig, F. Mansfeld, S. Tsai, *Corros. Sci*. 23 (1983) 317
39. A. Amirudin, D. Thieny, *Prog. Org. Coat*. 26 (1995) 1
40. Chunan Cao, Principles of Electrochemistry of Corrosion, Chemical Industry Press, Beijing, 2008
41. R. Lindström, L.-G. Johan, G.E. Thompson, P. Skeldon, J.-E. Svensson, *Corros. Sci*. 46 (2004), 1141